mathematics

Article

Solar Radiation and Thermal Convection of Hybrid Nanofluids for the Optimization of Solar Collector

Safyan Mukhtar [1,*] and Taza Gul [2]

[1] Department of Basic Sciences, Preparatory Year Deanship, King Faisal University, Al-Ahsa 31982, Saudi Arabia
[2] Department of Mathematics, City University of Science and Information Technology, Peshawar 25000, Pakistan
* Correspondence: smahmad@kfu.edu.sa

Abstract: This study aims to show the role of the stagnation point flow in solar optimization in the presence of a Riga plate. This requirement is conceivable in the case of solar energy management with a suitable solar collector covering and visual thermal optimization. Solar energy radiation and thermal convection of glycol ($C_3H_8O_2$)-based aluminum oxide (Al_2O_3) and copper (Cu) nanoparticles were used for a solar collector, and were studied in terms of the stagnation point flow theoretically. Stagnation refers to the state of a solar thermal system in which the flux varies in the collection loop to control the extra heating. The CVFEM code was used to analyze the flow in the case of represented stagnation using the FEA-Tools multiple physics software that manages partial derivative equations (PDEs). The streamlined patterns and energy contours for different cases were studied in detail. The transformation equations were treated with the numerical method (RK-4 technique) and showed strong agreement of the physical results corresponding to the initial conditions and boundaries. The results showed that hybrid nanofluids have the advanced capability to enhance the thermal performance of the base solvent and provide uniform distribution to the solar panel. The solar optimization and uniform thermal expansion results are displayed graphically.

Keywords: solar radiation; magnetic actuator with Riga plate; energy optimization by stagnation; hybridized nanofluid; CVFEM and RK-4 methods

MSC: 65N30

Citation: Mukhtar, S.; Gul, T. Solar Radiation and Thermal Convection of Hybrid Nanofluids for the Optimization of Solar Collector. *Mathematics* **2023**, *11*, 1175. https://doi.org/10.3390/math11051175

Academic Editor: Smirnov Nikolay Nikolaevich

Received: 2 February 2023
Revised: 23 February 2023
Accepted: 23 February 2023
Published: 27 February 2023

1. Introduction

To meet increasing collective energy needs, non-renewable energy sources are generally being used, which makes the environment dangerous and polluted. Non-renewable energy sources include fossil fuels, which have limited resources and low production, as well as causing climate change and smog in the atmosphere. To help reduce these drawbacks, systematic analysis can optimize the efficiency of renewable energies in the form of solar energy. The least expensive and most easily accessible renewable energy is solar, which can be converted into environmentally friendly electric and thermal energy. Using a heat transfer liquid, inclined solar panels are used to convert solar energy into thermal energy [1]. Solar collectors capture sunlight through the absorbing leaves and transfer heat to the absorbing solution (mainly a mixture of water and ethylene glycol). However, the main disadvantage is the low thermal properties of these traditional fluids due to their low thermal efficiency in the modification process. The replacement of the core work fluids with nanofluids is one of the processes that has gained interest in recent years to further improve the thermal efficiency of this technology. A stable solid material suspended at 1 nm to 100 nm is called a nanofluid [2]. A mono nanofluid is composed of a single material whose thermal expansion properties are restricted. Accordingly, a mixture of two/three different nanomaterials is used to improve the thermal properties of fluids and these are known as hybrid or tri-hybrid nanofluids [3]. The role of hybrid nanofluids and materials in several industrial applications is significant, such as heat exchangers [4], solar energy devices [5], flexible sheets [6], heat transfer [7,8], and photothermal conversion [9]. It has been found that the tri-hybrid nanofluid is more thermally conductive than the hybrid nanofluids and single kind of nanofluids using the heat transfer analysis of radiative Marangoni convective flow.

The relationship of hybrid nanofluids to stagnation has important applications in the solar energy sector, but flows in terms of stagnation point exist for fields other than solar energy, including almost all industrial, technological, and engineering fields. The main aspects of two-dimensional stagnation point fluid flow were pioneered and explained by Hiemenz [10] in 1911 through the use of similarity transformations.

Merkin [11] was the first to define the domain for physical conditions in the event of stagnant spot flow. In reality, from a physical point of view, stagnation has the greatest stress, heat transfer, and mass deposition [12]. Mat et al. [13] investigated the flow of the stagnation point under the influence of Joule heating, and viscous dissipation with slippery limits. Alghamdi et al. [14] examined the flow of the stagnation point using hybrid nanofluids to apply it to heat transfer. Gowda et al. [15] explained the idea of a Marangoni-based steady-state flow in a dusty nanofluid. Jamaludin et al. [16] investigated the mixed flow of stagnation points linked to the convection of leaves with suction and radiation phenomena.

The studies reviewed above found that the thermal conductivity of the hybrid type is greater than that of a single nanofluid. The heat capacity of the hybrid is shown to rise with accumulated temperature and decrease with declining volume fraction. Other significant investigations are included in the references of [17]. The parallel wall of Lorentz was created using an effective and competent method which was transformed into application using by Gailitis and Lielausis [18]. Permanent electrodes and magnets were presented as tables aligned in the direction of the range using an electromagnetic actuator produced through their use. This kind of geometry is recognized as the Riga plate [19]. The turbulence lowering and boundary layer separation procedure may be used to reduce the frictional force and drag of submarines. Saeed et al. [20] and Gul et al. [21] examined the nanofluid flow on a stretched surface. Iqbal et al. [22] considered the optimized rate of entropy on a Riga plate with an artificial lattice phenomenon. Shafiq et al. [23] explored nanotube flux on a Riga surface from the Marangoni boundary layer. Rasool et al. [24] reported the second-grade flow past a heated Riga surface. This research provides insights into topics related to stagnation and heat in general, and particularly for solar thermal applications. The main themes of this study are as follows.

- ❖ The primary purpose of this study is to investigate the stagnation and overheating of collectors and collection fields. Hybrid nanofluids containing $C_3H_8O_2$-based Al_2O_3 and Cu hybrid nanofluid are mentioned in [25]. The role of these types of materials with the existing Riga plate is valid and indicated in the aforementioned works. Therefore, we extend the idea to the solar energy system by looking at the stagnation point flux.
- ❖ The results obtained show that stagnation stabilizes the impact of heat consumption and heating control.
- ❖ To the best of our knowledge and conviction, the stagnation point flow on the Riga plate with some sort of flow configuration has not yet been studied.
- ❖ The solution of high non-linear problems relevant to heat and mass transfer was resolved by the researchers Tyurenkova and Smirnova [26] and Smirnova [27] using different numerical procedures. For the solution of the proposed model, the appropriate procedure was used.
- ❖ Specifically, the proposed model was solved using CVFEM [28–31] and the Runge–Kutta (RK-4) scheme [32–34].

2. Materials and Methods

A thermo-mechanical mathematical model was recently presented to investigate the effects of solar radiation on the free surface, considering the stagnation of the flow. The proposed model was formulated to address the associated coupled heat transfer problem, and fluid mechanics, in terms of the Riga plate. The previous study included nanofluid aspects in the presence of stagnation point, and the Riga plate, not in combination but separately investigated. Consequently, this study concentrated on the ability to model these terms together. The current work aimed to achieve nanofluid stagnation point hybrid phenomena of Cu and Al_2O_3 colloidal nanoparticle mixtures using $C_3H_8O_2$ base fluids surrounding the Riga plate. The model-building assumption, geometrical interpretation, and flow design are depicted in Figure 1a,b. Furthermore, a variable thermophysical model concerning viscosity and thermal conductivity was considered to stabilize solar radiation more appropriately. The simplified mathematical thermo-hybrid fluid model explored the application of physical parameters to solar thermal radiation, uniform flow distribution, thermal absorption, and optimization.

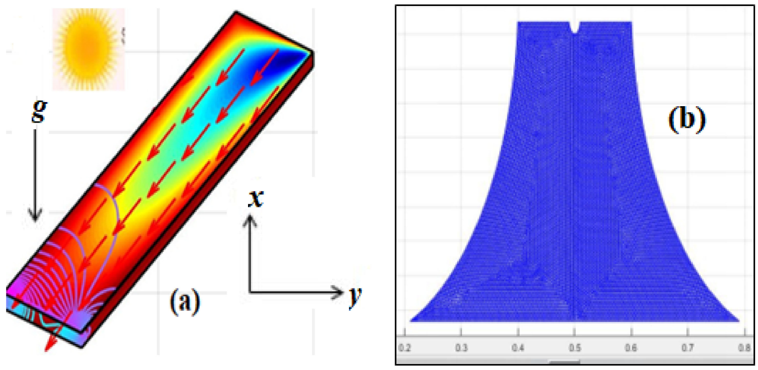

Figure 1. (**a**,**b**) Problem with geometry and grids.

Assumptions and Model Constraints

The mathematical model was observed to have the following presumptions and requirements:

- ❖ The Cu and Al_2O_3 nanoparticles were in thermal balance with the two core fluids.
- ❖ The source of energy, the dissipation effects, and the thermal radiation served to modify the thermal equations.
- ❖ The unsteady state of the flow was also taken into account.
- ❖ Using the T and Tw symbols, the free flow temperature and the plate surface were distinguished, respectively.

The base flow equations were regulated as in [10–13].

$$\frac{\partial u}{\partial x} + \frac{\partial v}{\partial y} = 0, \tag{1}$$

$$\frac{\partial u}{\partial t} + u\frac{\partial u}{\partial x} + v\frac{\partial u}{\partial y} = \frac{\partial u_e}{\partial t} + u_e\frac{\partial u_e}{\partial x} + v_{hnf}\frac{\partial^2 u}{\partial y^2} + \frac{g(\beta_T\rho)_{hnf}(T - T_\infty)}{\rho_{hnf}} + \left(\frac{\pi j_0 M_0}{8\rho_{hnf}}\right)e^{\left(\frac{-\pi y_1}{p}\right)}, \tag{2}$$

$$\frac{\partial T}{\partial t} + u\frac{\partial T}{\partial x} + v\frac{\partial T}{\partial y} = \frac{k_{hnf}}{(\rho c_p)_{hnf}}\left(\frac{\partial^2 T}{\partial y^2}\right) - \frac{1}{(\rho c_p)_{hnf}}\left(\frac{\partial q}{\partial y}\right) + \frac{\mu_{nf}}{(\rho c p)_{nf}}\left(\frac{\partial u}{\partial y}\right)^2. \tag{3}$$

The physical conditions were adjusted as follows:

$$\begin{aligned} u = u_0, v &= 0,\ T - T_w = 0, \ \text{at} \ y \to 0, \\ u - u_e = 0,&\ T - T_\infty = 0 \ \text{at} \ y \to \infty. \end{aligned} \tag{4}$$

The nanofluid density, dynamic viscosity, electrical conductivity, heat capacitance, and thermal conductivity are presented in the existing literature as $\rho_{nf},\ \mu_{nf}, \sigma_{nf}, (cp)_{nf}, k_{nf}$. The solar radiation term is defined as follows.

$$q = -\frac{4}{3}\frac{\sigma^*}{k^*}\frac{\partial T^4}{\partial y}, \tag{5}$$

Here, σ* and k^* are used to represent the Stefan–Boltzman constant and the mean absorption coefficient.

3. Transformations

The similarity variants are used as:

$$[u, v, \eta, \Theta,] = \left[u_0 + \frac{\alpha(x - x_0)}{t_{ref} - \beta t} f'(\eta), -\alpha\sqrt{\frac{v_f}{t_{ref} - \beta t}} f(\eta), \frac{y}{\sqrt{v_f\left(t_{ref} - \beta t\right)}}, \frac{T - T_\infty}{T_w - T_\infty},\right]. \tag{6}$$

$$f''' + \frac{\rho_{hnf}}{\rho_f}\frac{\mu_f}{\mu_{hnf}}\alpha\left[ff'' - (f')^2 + 1 - S\left(\frac{\eta}{2}f'' + f' - 1\right)\right] + \frac{\mu_f}{\mu_{hnf}}\mathrm{MH}\exp(-\Lambda\eta) = 0, \tag{7}$$

$$\left(\frac{k_{hnf}}{k_f} + \frac{4}{3}Rd\right)\Theta'' + \mathrm{Pr}\frac{(\rho cp)_{hnf}}{(\rho cp)_f}\left[\alpha f\Theta' - \frac{S\eta}{2}\Theta'\right] + \frac{\mu_f}{\mu_{hnf}}Ec(f')^2 = 0, \tag{8}$$

Transform physical conditions from (4) are distorted as:

$$f(0) = 0,\ f'(0) = c, \quad f'(\infty) = 1,\ \Theta(\infty) = 0, \Theta(0) = 1. \tag{9}$$

Note that in Equations (7)–(9), prime represents differentiation concerning η.

In this case, we were focusing on the shrinking sheet for which the value $(c < 0)$. If we consider the stretching case $(c = 1)$, then the solution is not possible because the ambient velocity also approaches 1, as stated in [10–14]. If we put $(c = 0)$, the solution will become Blasuis, as stated in [10], which is not our requirement. Therefore, our focus was on the $(c < 0)$ means shrinking sheet. The obtained dimensionless parameters are, accordingly, written below.

$$\begin{gathered} Rd = \frac{4\sigma^* T_\infty^3}{k^* k_f}, \mathrm{Pr} = \frac{\mu cp}{k_f}, S = \frac{\beta}{\alpha}, Ec = \frac{u_w^2}{(cp)_f(T_w - T_\infty)}, \\ \mathrm{Gr} = \frac{g(\beta_T)(T_w - T_\infty)x^3}{v_f^2}, \mathrm{MH} = \frac{\pi j_0 M_0}{8\alpha\rho_f}, \Lambda = \frac{\pi\sqrt{v_f}}{p}, \end{gathered} \tag{10}$$

where $\alpha > 0$, is a constant, known as the acceleration parameter.

Thermo-Physical Properties

Adding further for $\phi_{\mathrm{Cu}} = \phi_1,\ \phi_{\mathrm{Al_2O_3}} = \phi_2$, denoting the solid volume concentration of Cu & Al_2O_3, the relations used for the basic thermophysical characteristics of nanofluids are mentioned in Equation (11), whereas the numerical data are given in Table 1 below.

$$\begin{aligned}
&\frac{\rho_{hnf}}{\rho_f} = (1 - \phi_{\mathrm{Cu}})\left[(1 - \phi_{\mathrm{Al_2O_3}}) + \phi_{\mathrm{Al_2O_3}}\frac{\rho_{\mathrm{Al_2O_3}}}{\rho_f}\right] + \phi_{\mathrm{Cu}}\frac{\rho_{\mathrm{Cu}}}{\rho_f}, \frac{\mu_{hnf}}{\mu_f} = \frac{1}{(1 - \phi_{\mathrm{Cu}})^{2.5}(1 - \phi_{\mathrm{Al_2O_3}})^{2.5}}, \\
&\frac{(\rho cp)_{hnf}}{(\rho cp)_f} = (1 - \phi_{\mathrm{Cu}})\left[(1 - \phi_{\mathrm{Al_2O_3}}) + \phi_{\mathrm{Al_2O_3}}\frac{(\rho cp)_{\mathrm{Al_2O_3}}}{(\rho cp)_f}\right] + \phi_{\mathrm{Cu}}\frac{(\rho cp)_{\mathrm{Cu}}}{(\rho cp)_f}, \\
&\frac{\sigma_{hnf}}{\sigma_{nf}} = \frac{(1 + 2\phi_{\mathrm{Al_2O_3}})\sigma_{\mathrm{Al_2O_3}} + (1 - 2\phi_1)\sigma_{nf}}{(1 - \phi_{\mathrm{Al_2O_3}})\sigma_{\mathrm{Cu}} + (1 + \phi_{\mathrm{Al_2O_3}})\sigma_{nf}}, \frac{\sigma_{nf}}{\sigma_f} = \frac{(1 + 2\phi_{\mathrm{Cu}})\sigma_{\mathrm{Cu}} + (1 - 2\phi_{\mathrm{Cu}})\sigma_f}{(1 - \phi_{\mathrm{Cu}})\sigma_{\mathrm{Cu}} + (1 + \phi_{\mathrm{Cu}})\sigma_f}, \\
&\frac{k_{hnf}}{k_{nf}} = \left(\frac{k_{\mathrm{Al_2O_3}} + 2k_{nf} - 2\phi_{\mathrm{Al_2O_3}}\left(k_{nf} - k_{\mathrm{Al_2O_3}}\right)}{k_{\mathrm{Al_2O_3}} + 2k_{nf} + \phi_{\mathrm{Al_2O_3}}\left(k_{nf} - k_{\mathrm{Al_2O_3}}\right)}\right), \frac{k_{nf}}{k_f} = \left(\frac{k_{\mathrm{Cu}} + 2k_f - 2\phi_{\mathrm{Cu}}\left(k_f - k_{\mathrm{Cu}}\right)}{k_{\mathrm{Cu}} + 2k_f + \phi_{\mathrm{Cu}}\left(k_f - k_{\mathrm{Cu}}\right)}\right),
\end{aligned} \tag{11}$$

Table 1. Various thermophysical features of base liquids and nanoparticles.

Physical Features	Al_2O_3	Cu	$C_3H_8O_2$
$k(W/mK)$	40	400	34.5
$c_p(J/Kg\,K)$	765	385	4338
$\rho(Kg/m^3)$	3970	8933	5060
$\sigma(s/m)$	35×10^6	59.6×10^6	0.5×10^6
$\beta(1/k)$	0.85	1.67	0.00062

4. Simulation for Cu-Al_2O_3/$C_3H_8O_2$ Hybrid Nanofluid

The proposed models of μ_{hnf} and k_{hnf} for Cu-$Al_2O_3/C_3H_8O_2$ are extended using the idea [35] from nanofluid to hybrid nanofluid as follows.

$$\begin{aligned} \frac{\mu_{hnf}}{\mu_f} &= (306\phi_{\mathrm{Cu}}^2 - 0.19\phi_{\mathrm{Cu}} + 1)(306\phi_{\mathrm{Al_2O_3}}^2 - 0.19\phi_{\mathrm{Al_2O_3}} + 1), \\ \frac{k_{hnf}}{k_f} &= (306\phi_{\mathrm{Cu}}^2 - 0.19\phi_{\mathrm{Cu}} + 1)(306\phi_{\mathrm{Al_2O_3}}^2 - 0.19\phi_{\mathrm{Al_2O_3}} + 1). \end{aligned} \tag{12}$$

Physical Quantities

Following are the focused physical quantities, i.e., drag force and rate of heat transfer.

$$Cf = \frac{\tau_w}{\rho_{hnf} u_e^2}, \tau_w = \mu_{hnf}\left(\frac{\partial u}{\partial y}\right)_{y=0}, Nu_x = \frac{x q_w}{k_f(T_w - T_0)}, q_w = -\left[k_{hnf} + \frac{16\sigma^* T_\infty^3}{3k^*}\right]\left(\frac{\partial T}{\partial y}\right)_{y=0}, \tag{13}$$

The non-dimensional forms of Cf $\&Nu_x$ are as follows.

$$R_e^{0.5} Cf = \left(\frac{\mu_{hnf}}{\mu_f}\right) f''(0),\ R_e^{-0.5} Nu_x = -\left(\frac{k_{hnf}}{k_f} + \frac{4}{3} Rd\right)\Theta'(0). \tag{14}$$

5. Solution Methodologies

The accuracy of the current work program was further assessed by equalizing the numerical and graphical results using numerical tools like the control volume finite element method (CVFEM) [28–31] and the Runge–Kutta (RK-4) scheme [32,33]. CVFEM is a newly developed technique aimed at obtaining a reliable numerical solution of the nonlinear system of partial differential equations. The CVFEM method uses the two advantages of two common CFD methods. It uses a triangular member as shown in [31]. A wind approach is used for advection. The Gauss–Seidel approach is applied to solving ultimate algebraic equations. For further details, refer to [31]. The results should not depend upon the size of the cells. As a result, several grids need to be tested. For instance, it is possible to select a grid size of 72×232. That this CVFEM code provides good accuracy for stagnation point flow has been shown physically.

5.1. Discussion

Numerous physical fluid parameters have the most important consequences upon non-dimensionalized properties and are shown high consideration in this phase. Because of the above considerations, the parameters Gr, M_H, Λ, ϕ, Rd, Ec, and S have significantly vigorous effects on respective diffusivity. The impacts on the dimensionless velocity ($f'(\eta)$) and temperature ($\Theta(\eta)$) profiles in opposition to essential parameters are illustrated in Figures 2 and 3 respectively. Moreover, CVFEM simulates various physical characteristics of flow phenomena, as illustrated by Figures 4–8. On the other hand, the numerical evaluations from RK-4 are reported in Table 2.

5.2. Analysis of Velocity and Temperature Profiles

The nanocomposite-based hybrid fluid notably improved the energy diffusion ratio as compared to the nanofluid alone. Physically, the objective of the creation of nanofluid mixtures is to improve the qualities of the individual nanoparticles by giving them an improved rheological or thermal conductivity. The thermal effectiveness of the nano liquid produced can be improved by the formation of a compound nanocomposite. This is done by creating an ideal mixture of nanocrystals. A higher heat conductivity does not necessarily imply better rheological properties in a nanofluid created by the addition of nanoparticles. Therefore, improving the overall capacity of the nanofluid and making it more stable and efficient can be achieved by including nanoparticles with various rheological or thermodynamical properties. Al_2O_3, for instance, has moderate thermal conductivity while demonstrating notable chemical inertia and longevity. However, materials with a higher thermal conductivity, such as aluminum, silver, copper, silica, and titanium, are unstable and chemically reactive. Consequently, hybrids are created by blending these nanomaterials with various physical and chemical links. These nanofluids are widely used in the pharmaceutical sector, electrical radiator cooling, nuclear safety, and other areas. Keeping c = −0.5, the plots of Figure 2a−d display the various impacts of fluid velocity $f'(\eta)$ against variations in Gr, M_H, ϕ and Λ, respectively. From Figure 2a,b, it can be seen that $f'(\eta)$ shows quite progressive responses regarding increasing values for both Gr and M_H. On the contrary, opposite behaviors are observed when the measures for ϕ and Λ undergo increases, as plotted in Figure 2c,d. Furthermore, it is also evident from all the schematics of Figure 2 that the results recorded somewhat intensified in the case of nanofluid in comparison to that of hybrid nanofluid; however, the consequences with increments in ϕ varied only very slightly in both scenarios.

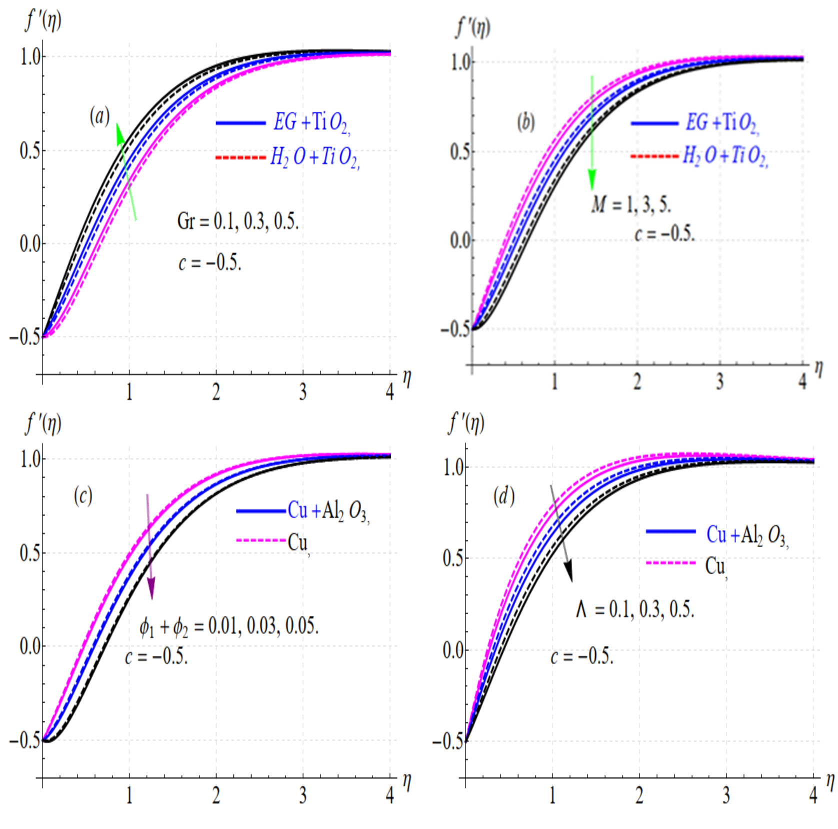

Figure 2. (**a–d**) Influence of Gr, M_H, ϕ, and Λ vs. $f'(\eta)$, keeping c = −0.5.

On the other hand, the graphics in Figure 3 display the ramifications resulting for $\Theta(\eta)$ against increments in Ec, Rd, ϕ, and S, separately. Figure 3a explicitly portrays the influence of Ec on dimensionless temperature for both ascending and descending cases. It is found that Θ(η) has major constructive impacts for increasing yet positive Ec > 0. From a physics perspective, the Eckert number is a measure of the difference between the thermodynamic states of the fluid and the wall, which provides information about the self-heating characteristics of the fluid in high-speed environments.

Due to the viscous interactions between fluid layers, frictional heat dissipates as Ec increases, intensifying the fluid's temperature. The Eckert number is the relationship of kinetic energy to the specific enthalpy alteration between the wall and the fluid. Therefore, an increase in the value of Eckert causes the transformation of kinetic energy into internal energy by the work which is made against the viscous fluid constraints.

The Eckert number is used to describe the influence of the self-heating of fluid after dissipating effects. In the case of a high flow rate, the dissipation is caused by the internal colloidal forces of the fluid and, as a result, the thermal field of a fluidic system is increased due to the internal heating of the fluids. In addition, temperature gradients control the thermal field and accordingly self-heating causes changes in the temperature profile to improve with an increase in the Eckert number. Despite that, the destructive notion is perceived as contrary to Ec < 0. Similarly, negative values for the Eckert number provide cooling performance and decrease the temperature profile. This fluctuation in the thermal profile makes it possible to optimize and stabilize the solar collector. In Figure 3b,c, it is accordingly implied that Θ(η) is the increasing function of thermal radiation and nanoparticles concentration. Solar radiation enhances the thermal profile to increase Rd values. The selected range of the radiation parameter was adjusted for the stabilization and convergence of the problem of the proposed model. The increasing amount of the solid nanoparticle volume fraction improved the thermal efficiency of the base fluid and, consequently, the thermal field was enhanced. Nevertheless, increasing values of S cause a decline in temporal ranges, as is visible in Figure 3d. Moreover, just as in the case of fluid velocity (see Figure 2), it is also evident from Figure 3 that the influential factors demonstrate significant support for using Al_2O_3+Cu rather than Cu.

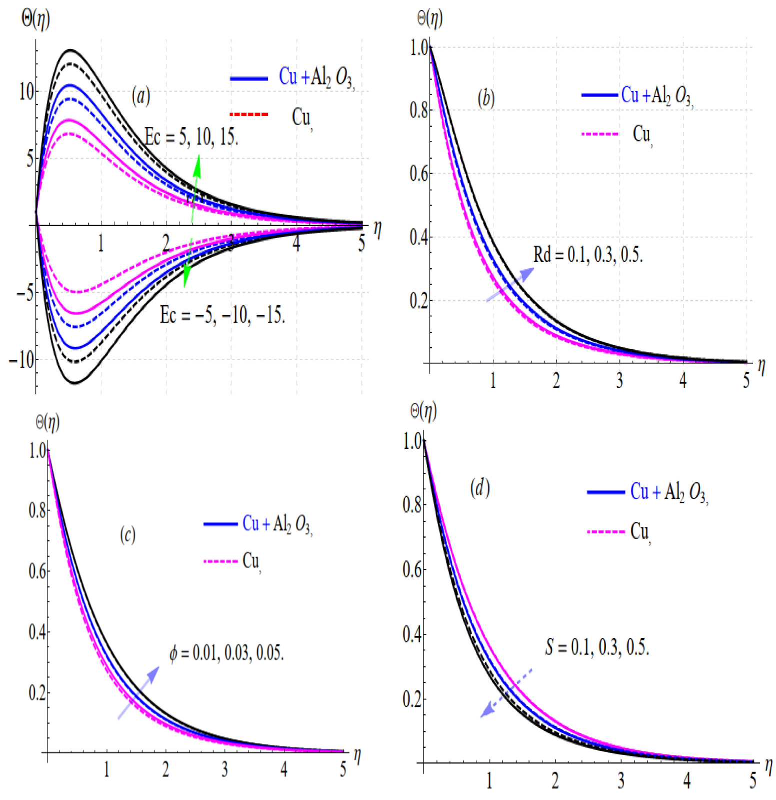

Figure 3. (**a**–**d**). Influence of Ec, Rd, ϕ and S vs. Θ(η).

5.3. Analysis of CVFEM Results

The visuals in Figure 5 elucidate the repercussions of the fluid's motion and magnetic field. Two contexts are considered to simulate the results, for which Figure 4a–d show the CVFEM views in parts and as a whole for the used characteristics. The contours of velocity are framed in Figure 4a, while Figure 4b–d separately manifest the magnetic profiles. Figure 4b–d show that increasing values of the Hartmann number improve the magnetic effect more manifestly.

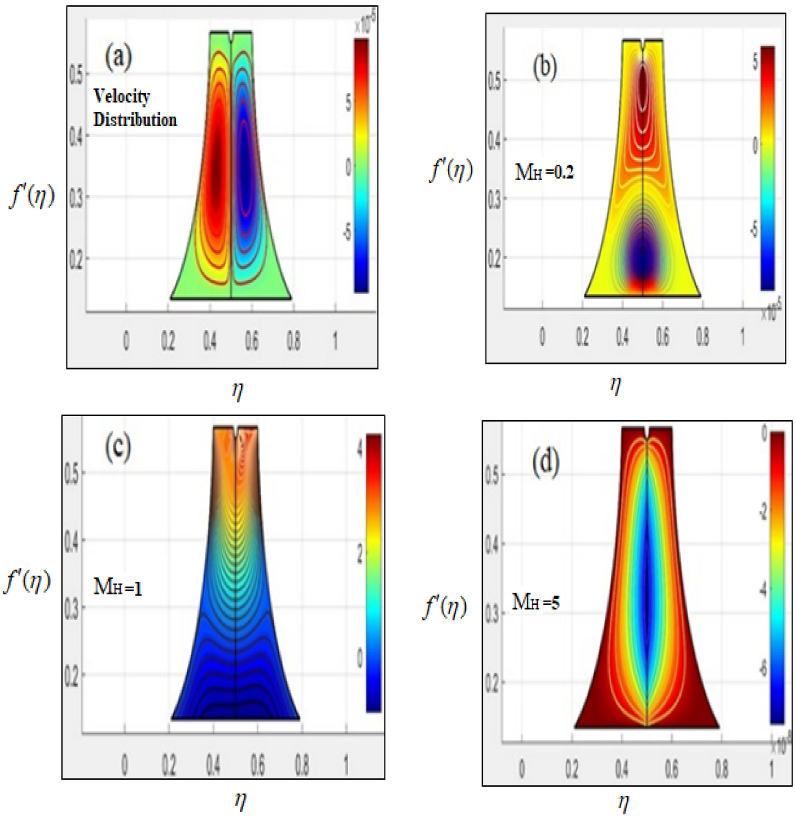

Figure 4. CVFEM: partial and overall views of fluid motion and magnetic field.

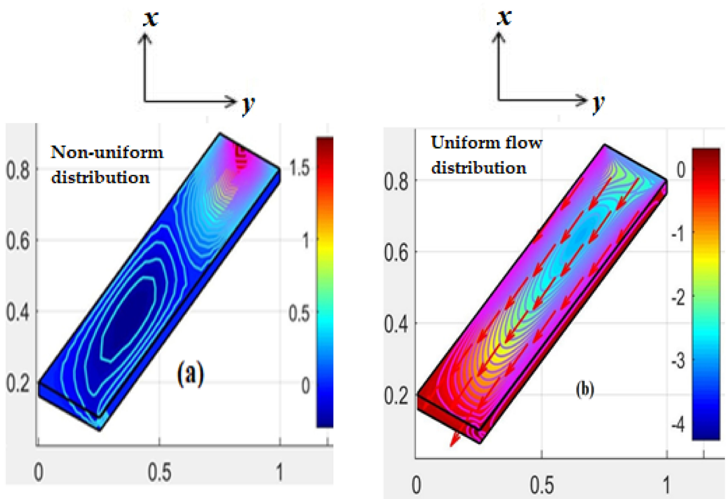

Figure 5. Stream contour of the fluid distribution over the solar panel (**a**) not uniform, (**b**) unifrom.

The Al_2O_3-Cu hybrid nanofluid flow distribution is shown in Figure 5a,b. In Figure 6a, the flow distribution is not uniform, indicating that the panel is not favorable for maximum thermal energy gain. The adjustment required for the uniform distribution is possible through machine learning software, as shown in Figure 5b. In addition, the consequences faced by skin friction in opposition to Gr = 0.1, 0.2, 0.4, 0.6, and ϕ = 0.01, 0.02, 0.03, 0.04, can be understood from plots Figure 6a,b respectively.

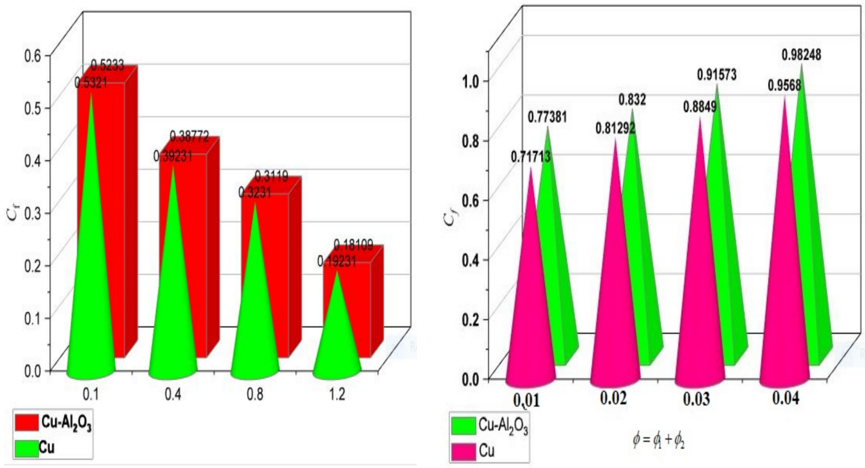

(**a**) (**b**)

Figure 6. C_{f_z} subject to (**a**) Gr and (**b**) ϕ.

It is observed that C_{f_z} declines against higher measures of Gr, whereas, on the contrary, ϕ sees improved results with C_{f_z}. Likewise, the aftereffects of M_H = 0.1, 0.3, 0.7, 0.9 and Rd = 0.1, 0.3, 0.5, 0.7 on the Nusselt number are graphically explained in Figure 7a,b, respectively. Nu_z undergoes gradual enhancements under increasing M_H, while favorably intensifying against solar radiation.

In the view of thermo-fluid-dynamics, the Nusselt number denotes the ratio of convective to conductive heat transfer at a fluid boundary. Therefore, we deduced that convective thermal transport is the better option for higher solar radiation in comparison to heat conduction. The plots in Figures 7 and 8 also show a comparative analysis between nanofluid and hybrid nanofluid. It is notable that all the above improvements are recorded with enhancements for hybrid nanofluid, since hybrid nanoparticles have more thermal response compared to mono nanoparticles. Figure 8 indicates the percentage-wise comparison of the nanoparticle volume fraction and heat transfer. It can be seen that hybrid nanofluids (Cu-Al_2O_3) are more effective than the (Cu) nanofluid.

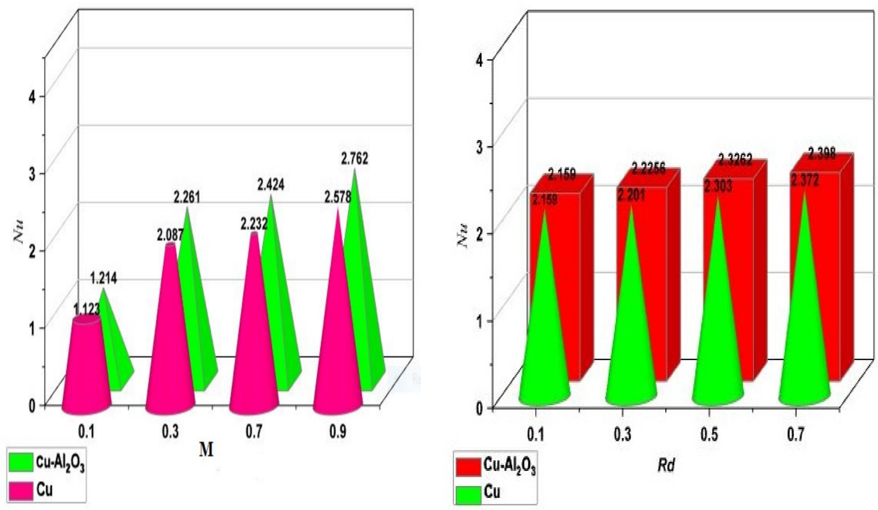

(**a**) (**b**)

Figure 7. Nu_z subject to M and Rd. (**a**) Effect of M. (**b**) Effect of Rd.

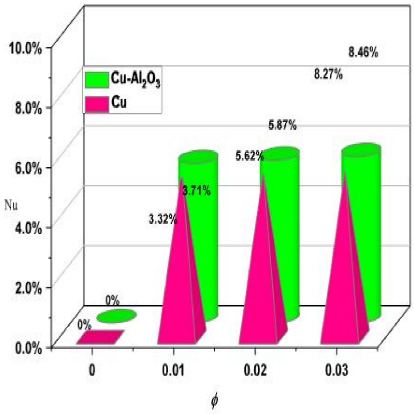

Figure 8. Percentage-wise comparison between ϕ and heat transfer.

5.4. Analysis of Numerical Results

A numeric comparison for skin friction $f''(0)$ is shown in Table 2 against different values of the acceleration parameter $\alpha = \frac{a}{b}$ and keeping the rest of the parameters unvarying. The results of Wang [12], Ishak et al. [35], and Lok and Pop [36] are also presented side by side in columns. As a result, a successful concurrence is seen among the abovementioned data. Moreover, it is observed that $f''(0)$ sees a rise for $\alpha < 0$, though improvements are also seen for positive ranges.

Table 2. Skin friction validation compared to published work based on common parameters.

	Wang [12]	**Ishak et al. [36]**	**Lok and Pop [37]**	**[Present]**
$\alpha = \frac{a}{b}$	$f''(0)$	$f''(0)$	$f''(0)$	$f''(0)$
−2.0	0.132762176	0.13278657	0.133573201	0.1336832065
−1.5	0.321752183	0.321764321	0.3221033254	0.3221033254
−1.0	1.372174420	1.372183216	1.3733109750	1.37342298342
−0.5	1.5120132321	1.5120265437	1.5131023204	1.51321321032
0	1.342175542	1.342276489	1.3431230281	1.34323321084
0.5	0.82451314	0.824665432	0.8251202013	0.82522321087
1.0	0	0	0	0
1.5	−1.215424321	−1.215552107	−1.2141203201	−1.2142134265
2.0	−1.898423214	−1.898533210	−1.8972312935	−1.8973413287

6. Conclusions

How the stagnation point flux plays an important role in the application of solar optimization is the main aim of this research. The CVFEM and RK-4 methods were applied to compute and analyze the model problems. The results obtained were validated using previously published results, taking into account the common parameters and not mentioning the new parameters. The CVFEM code was used to analyze flow in case of stagnation and represented using FEA-Tools multiple physics software handling the PDEs. The streamlined patterns and energy contours for different cases were studied in detail. The transformation equations were treated with the numerical method (RK-4 technique) and showed strong agreement of the physical results corresponding to the initial conditions and boundaries. This study led to the following conclusions:

- ➢ Inclusion of the Riga plate concept enhanced the heat transfer effect and its application for the optimization of solar energy was also predicted.
- ➢ During the stagnation flow, phenomena acceleration was detected for the higher values of Gr. In addition, the range of the Gr was observed to optimize and control the stable flow phenomena.

- ➢ Raising both M and ϕ_{TiO_2} had favorable aftereffects on the Nusselt number, although their influences on skin friction are not much appreciated.
- ➢ It was observed that solar panel adjustment is also necessary for uniform solar radiation absorption, as seen in Figure 6.
- ➢ It was observed that the single kind of nanoparticles had a limited capacity to enhance the thermal field as compared to the hybrid nanofluid which had more intense outcomes in thermal performance.
- ➢ The percentage-wise enhancement, as shown in Figure 8, proved that the hybrid nanofluids are more promising than the single kind of nanofluids in the field of thermal engineering and solar energy devices.

Author Contributions: Methodology, T.G.; Software, S.M. and T.G.; Validation, T.G.; Formal analysis, T.G.; Investigation, S.M.; Resources, S.M. and T.G.; Writing—review & editing, S.M. All authors have read and agreed to the published version of the manuscript.

Funding: The authors extend their appreciation to the Deputyship for Research and Innovation, Ministry of Education in Saudi Arabia, for funding this research work through the Project number INST135.

Data Availability Statement: All the relevant data exist in the manuscript.

Acknowledgments: The authors extend their appreciation to the Deputyship for Research and Innovation, Ministry of Education in Saudi Arabia, for funding this research work through the Project number INST135.

Conflicts of Interest: The authors do not have any conflict of interest.

Nomenclature

List of symbols	
u, v	Components of velocity $\left(ms^{-1}\right)$.
j_0	Applied current density of the electrodes
u_e	Stagnation velocity $\left(ms^{-1}\right)$.
MH	Modified Hartmann number
M_0	Magnetization of the magnets
Re	Reynold number
Ec	Eckert number
Gr	Thermal Grashof number
S	Unsteady term
g	Gravitational acceleration
Θ, f	Dimensional thermal, velocity fields
T	Temperature of fluid (K).
T_w, T_∞	Lower, upper wall temperature (K).
Pr	Prandtl number
Greek symbols	
μ_{hnf}	Viscosity of hybrid nanofluid (mPa).
β_T	Thermal expansion
Rd	Solar radiation factor
Λ	Dimensionless parameter
η	Dimensionless transform variable
α	Stretching shrinking parameter
cp_{hnf}	Heat capacitance of hybrid nanofluid
cp_f	Heat capacitance of base liquid
μ_f	Viscosity of the base fluid (mPa).
k_{hnf}	Thermal conductivity
ρ_{hnf}	Hybrid nanofluid density $\left(Kgm^{-3}\right)$.
ρ_f	Base fluid density $\left(Kgm^{-3}\right)$.
σ_{nf}	Electrical conductivity
ϕ	Nanoparticle volume fraction

References

1. Rejeb, O.; Yousef, M.S.; Ghenai, C.; Hassan, H.; Bettaye, M. Investigation of a solar still behaviour using response surface methodology. *Case Stud. Therm. Eng.* **2021**, *24*, 100816. [CrossRef]
2. Choi, U.S. Enhancing thermal conductivity of fluids with nanoparticles. *AS-MEFED* **1995**, *231*, 99–103.
3. Atashafrooz, M.; Sajjadi, H.; Delouei, A.A. Simulation of Combined Convective-Radiative Heat Transfer of Hybrid Nanofluid Flow inside an Open Trapezoidal Enclosure Considering the Magnetic Force Impacts. *J. Magn. Magn. Mater.* **2023**, *1*, 170354. [CrossRef]
4. Khan, A.; Kumam, W.; Khan, I.; Saeed, A.; Gul, T.; Kumam, P.; Ali, I. Chemically reactive nanofluid flow past a thin moving needle with viscous dissipation, magnetic effects and hall current. *PLoS ONE* **2021**, *16*, e0249264. [CrossRef]
5. Amiri Delouei, A.; Karimnejad, S.; Gharajeh, A.; Sajjadi, H.; Atashafrooz, M.; Xie, G.; Arabkoohsar, A. Bath heaters using alternative heat transfer medium: A thermo-economic analysis. *J. Braz. Soc. Mech. Sci. Eng.* **2023**, *45*, 73. [CrossRef]
6. Manjunatha, S.; Puneeth, V.; Gireesha, B.J.; Chamkha, A. Theoretical study of convective heat transfer in ternary nanofluid flowing past a stretching sheet. *J. Appl. Comput. Mech.* **2022**, *8*, 1279–1286.
7. Islam, Z.; Taza, G.; Dosmagulova, K.; Khan, T.S.; Safia, H. Heat transfer analysis of Radiative-Marangoni Convective flow in nanofluid comprising Lorentz forces and porosity effects. *Adv. Theory Nonlinear Anal. Its Appl.* **2023**, *7*, 61–81.
8. Naveen Kumar, R.; Suresh Goud, J.; Srilatha, P.; Manjunatha, P.T.; Rani, S.P.; Kumar, R.; Suresha, S. Cattaneo–Christov heat flux model for nanofluid flow over a curved stretching sheet: An application of Stefan blowing. *Heat Transf.* **2022**, *51*, 4977–4991. [CrossRef]
9. Li, Z.; Kan, A.; Wang, K.; He, Y.; Zheng, N.; Yu, W. Optical properties and photothermal conversion performances of graphene based nanofluids. *Appl. Therm. Eng.* **2022**, *203*, 117948. [CrossRef]
10. Hiemenz, K. The boundary layer on a straight circular cylinder immersed in the uniform flow of liquid. *Dinglers Polytech. J.* **1911**, *326*, 321–324.
11. Merkin, J.H. On dual solutions occurring in mixed convection in a porous medium. *J. Eng. Math.* **1986**, *20*, 171–179. [CrossRef]
12. Wang, C.Y. Stagnation flow towards a shrinking sheet. *Int. J. Non-Linear Mech.* **2008**, *43*, 377–382. [CrossRef]
13. Mat Yasin, M.H.; Ishak, A.; Pop, I. MHD stagnation-point flow and heat transfer with effects of viscous dissipation, Joule heating and partial velocity slip. *Sci. Rep.* **2015**, *5*, 1–8. [CrossRef] [PubMed]
14. Alghamdi, W.; Gul, T.; Nullah, M.; Rehman, A.; Nasir, S.; Saeed, A.; Bonyah, E. Boundary layer stagnation point flow of the Casson hybrid nanofluid over an unsteady stretching surface. *AIP Adv.* **2021**, *11*, 015016. [CrossRef]
15. Gowda, R.P.; Mallikarjuna, H.B.; Prasannakumara, B.C.; Kumar, R.N.; Manjunatha, P.T. Dynamics of thermal Marangoni stagnation point flow in dusty Casson nanofluid. *Int. J. Model. Simul.* **2022**, *42*, 707–715. [CrossRef]
16. Jamaludin, A.; Nazar, R.; Pop, I. Mixed convection stagnation-point flow of Cross fluid over a shrinking sheet with suction and thermal radiation. *Phys. A Stat. Mech. Appl.* **2022**, *585*, 126398. [CrossRef]
17. Zari, I.; Ali, F.; Khan, T.S.; Shafiq, A. Radiative Hiemenz flow towards a stretching Riga plate in hybrid nanofluids. *Int. Commun. Heat Mass Transf.* **2022**, *139*, 106492. [CrossRef]
18. Gailitis, A.; Lielausis, O. On a possibility to reduce the hydrodynamic resistance of a plate in an electrolyte. *Appl. Magnetohydrodyn.* **1961**, *12*, 143–146.
19. Waini, I.; Ishak, A.; Pop, I. Symmetrical solutions of hybrid nanofluid stagnation-point flow in a porous medium. *Int. Commun. Heat Mass Transf.* **2022**, *130*, 105804. [CrossRef]
20. Saeed, A.; Bilal, M.; Gul, T.; Kumam, P.; Khan, A.; Sohail, M. Fractional order stagnation point flow of the hybrid nanofluid towards a stretching sheet. *Sci. Rep.* **2022**, *11*, 20429. [CrossRef] [PubMed]
21. Gul, T.; Ali, B.; Alghamdi, W.; Nasir, S.; Saeed, A.; Kumam, P.; Jawad, M. Mixed convection stagnation point flow of the blood based hybrid nanofluid around a rotating sphere. *Sci. Rep.* **2021**, *11*, 7460. [CrossRef] [PubMed]
22. Iqbal, Z.; Khan, M.; Shoaib, M.; Matoog, R.T.; Muhammad, T.; El-Zahar, E.R. Study of buoyancy effects in unsteady stagnation point flow of Maxwell nanofluid over a vertical stretching sheet in the presence of Joule heating. *Waves Random Complex Media* **2022**, *1*, 1–15. [CrossRef]
23. Shafiq, A.; Zari, I.; Khan, I.; Khan, T.S.; Seikh, A.H.; Sherif, E.S.M. Marangoni driven boundary layer flow of carbon nanotubes toward a Riga plate. *Front. Phys.* **2020**, *7*, 215. [CrossRef]
24. Rasool, G.; Zhang, T.; Shafiq, A. Second grade nanofluidic flow past a convectively heated vertical Riga plate. *Phys. Scr.* **2019**, *94*, 125212. [CrossRef]
25. Khan, U.; Zaib, A.; Ishak, A.; Waini, I.; Abdel-Aty, A.H.; Sheremet, M.A.; Galal, A.M. Agrawal Axisymmetric Rotational Stagnation-Point Flow of a Water-Based Molybdenum Disulfide-Graphene Oxide Hybrid Nanofluid and Heat Transfer Impinging on a Radially Permeable Moving Rotating Disk. *Nanomaterials* **2022**, *12*, 787. [CrossRef]
26. Tyurenkova, V.V.; Smirnova, M.N. Material combustion in oxidant flows: Self-similar solutions. *Acta Astronaut.* **2016**, *120*, 129–137. [CrossRef]
27. Smirnov, N.N. Heat and mass transfer in a multi-component chemically reactive gas above a liquid fuel layer. *Int. J. Heat Mass Transf.* **1985**, *28*, 929–938. [CrossRef]
28. Hamilton, R.L.; Crosser, O.K. Thermal conductivity of heterogeneous two-component systems. *Ind. Eng. Chem. Fundam.* **1962**, *1*, 187–191. [CrossRef]

29. Wang, H.F.; Anderson, M.P. *Introduction to Groundwater Modeling: Finite Difference and Finite Element Methods*; Academic Press: Cambridge, MA, USA, 1995.
30. Reddy, J.N. *Introduction to the Finite Element Method*; McGraw-Hill Education: New York, NY, USA, 2019.
31. Li, H. The finite element method. In *Graded Finite Element Methods for Elliptic Problems in Nonsmooth Domains*; Springer: Cham, Switzerland, 2022; pp. 1–12.
32. Zhou, L.; Wang, J.; Liu, M.; Li, M.; Chai, Y. Evaluation of the transient performance of magneto-electro-elastic based structures with the enriched finite element method. *Compos. Struct.* **2022**, *280*, 114888. [CrossRef]
33. Bakir, Y.; Mert, O. On solution of ordinary differential equations by using HWCM, ADM and RK4. *Int. J. Mod. Phys. C* **2022**, *2*, 2250135. [CrossRef]
34. Zainal, N.A.; Nazar, R.; Naganthran, K.; Pop, I. Magnetic Impact on the Unsteady Separated Stagnation-Point Flow of Hybrid Nanofluid with Viscous Dissipation and Joule Heating. *Mathematics* **2022**, *10*, 2356. [CrossRef]
35. Salawu, S.O.; Obalalu, A.M.; Okoya, S.S. Thermal convection and solar radiation of electromagnetic actuator Cu–Al2O3/C3H8O2 and Cu–C3H8O2 hybrid nanofluids for solar collector optimization. *Mater. Today Commun.* **2022**, *33*, 104763. [CrossRef]
36. Ishak, A.; Lok, Y.Y.; Pop, I. Stagnation-point flow over a shrinking sheet in a micropolar fluid. *Chem. Eng. Commun.* **2010**, *197*, 1417–1427. [CrossRef]
37. Lok, Y.Y.; Pop, I. Stretching or shrinking sheet problem for unsteady separated stagnation point flow. *Meccanica* **2014**, *49*, 1479–1492. [CrossRef]